Nano Energy 58 (2019) 11–22

Contents lists available at ScienceDirect

Nano Energy

journal homepage: www.elsevier.com/locate/nanoen

Full paper

Synthesis and characterization of nanofiber-type hydrophobic organic materials as electrodes for improved performance of PVDF-based piezoelectric nanogenerators

Eui Jin Ko[a], Sung Jae Jeon[a], Yong Woon Han[a], Se Yeong Jeong[b], Chong Yun Kang[c,d], Tae Hyun Sung[b], Kee Won Seong[e], Doo Kyung Moon[a,*]

[a] Department of Chemical Engineering, College of Engineering, Konkuk University, 1 Hwayang-dong, Gwangjin-gu, Seoul 05029, Republic of Korea
[b] Department of Electrical Engineering, Hanyang University, 222 Wangsimni-ro, Seongdong-gu, Seoul 04763, Republic of Korea
[c] KU-KIST Graduate School of Converging Science and Technology, Korea University, Seoul 02841, Republic of Korea
[d] Center for Electronic Materials, Korea Institute of Science and Technology, Seoul 02792, Republic of Korea
[e] Department of Civil Engineering, College of Engineering, Konkuk University, 1 Hwayang-dong, Gwangjin-gu, Seoul 05029, Republic of Korea

ARTICLE INFO

Keywords:
Poly(3,4-ethylenedioxythiophene) derivative
Nanofiber
Hydrophobicity
Nanofibrillar network
Piezoelectric nanogenerator

ABSTRACT

Poly(3,4-ethylenedioxythiophene) (PEDOT) derivatives are synthesized by oxidative polymerization using sodium dodecyl sulfate (SDS) as an anionic surfactant dopant. The resulting polymeric materials featuring nanofiber-type one-dimensional (1D) structures are identified as poly(2-butyl-2,3-dihydrothieno[3,4-b][1,4]dioxine:dodecyl sulfate (PEDOT-C_4:DS) and poly(2-hexyl-2,3-dihydrothieno[3,4-b][1,4]dioxine:dodecyl sulfate (PEDOT-C_6:DS). The ratio of the DS anion doped into PEDOT-C_4:DS and PEDOT-C_6:DS is 0.16 and 0.23, respectively. The contact angle of water on the PEDOT-C_4:DS and PEDOT-C_6:DS films is 76.6° and 87.7°, respectively, showing hydrophobic properties similar to that with water on PVDF. It facilitated the fully uniform film formation due to excellent surface matching. Peeling force of PEDOT-C_4:DS and PEDOT-C_6:DS is stronger than the one of PEDOT:PSS-CNT composite. GIWAX analysis showed that PEDOT-C_4:DS formed the highly ordered edge-on structure and PEDOT-C_6:DS formed the bimodal orientation consisting of edge-on structure mainly and face-on structure slightly. The electrical conductivity ($\sigma_{PEDOT\text{-}C4:DS} = 50.0\ S\ cm^{-1}$) of PEDOT-$C_4$:DS is 41.7 times higher than that of PEDOT:PSS ($\sigma_{PEDOT:PSS} = 1.2\ S\ cm^{-1}$).

The output signals (maximum voltages/currents) of piezoelectric nanogenerators (PNGs, electrode/PVDF/electrode) using these materials as electrodes are PNG-1 (PEDOT:PSS-CNT composite) 1.25 V/128.5 nA, PNG-2 (PEDOT-C_4:DS) 1.54 V/166.0 nA, and PNG-3 (PEDOT-C_6:DS) 1.49 V/159.0 nA. Of these, PNG-2 & PNG-3 show maximum piezoelectric output power of 63.0 nW and 59.9 nW at 9 MΩ compared to PNG-1 (41.0 nW at 10 MΩ). They are enhanced up to 53.7%. The excellent surface matching between a piezoelectric active material and an electrode material leads to high output power.

1. Introduction

The 4th Industrial Revolution has greatly stimulated demands for portable and self-powered electronics, such as mobile electronics, wireless devices and medical sensors. As a result, various fields are now vigorously researching into self-powered system. In this current trend, low-power energy harvesting technologies using natural energy, such as mechanical, solar, and thermal energy, have been spotlighted [1–7]. Of these, a subject attracting substantial attention is piezoelectric nanogenerators (PNGs), which convert mechanical energy, such as human movements, various vibrations, and wind flow, into electrical energy.

PNGs offer a range of benefits for small electronic devices because they are eco-friendly, have fewer restrictions on operating environments and are self-chargeable [8]. PNGs essentially consist of 1) inorganic or organic piezoelectric materials and 2) electrodes in a sandwich-type structure.

1) Inorganic materials such as zinc oxide (ZnO), lead zirconate-titanate (PZT), and barium titanate ($BaTiO_3$) are excellent hydrophilic materials featuring a high piezoelectric output performance [9–12]. However, limitations exist regarding the application of the above-mentioned materials in various fields due to their high temperature

* Corresponding author.
E-mail address: dkmoon@konkuk.ac.kr (D.K. Moon).

https://doi.org/10.1016/j.nanoen.2019.01.022
Received 12 July 2018; Received in revised form 5 January 2019; Accepted 7 January 2019
Available online 08 January 2019
2211-2855/

requirement, complex processes, poor flexibility and brittleness. Ferroelectric polymers, such as poly(vinylidene fluoride) (PVDF) and poly(vinylidenefluoride-co-trifluoroethylene) (P(VDF-TrFE)), feature relatively low piezoelectric performance and hydrophobicity compared to inorganic piezoelectric materials. However, the light weight and good flexibility of these materials are key to further research and the development of a number of flexible devices [13–18].

2) The majority of electrodes used for piezoelectric devices, such as gold (Au), silver (Ag), copper (Cu), and indium tin oxide (ITO), are hydrophilic and rigid. Therefore, hydrophobic organic piezoelectric materials, such as PVDF, have the critical disadvantage of poor surface contact with these electrodes. Devices are easily cracked when deformed, and breakage occurs due to the poor adhesiveness, which results in poor durability [19].

For flexible PNGs, metallic nanowires, such as silver nanowires (AgNWs), or organic conductive materials, such as poly(3,4-ethylenedioxythiophene):polystyrene sulfonate (PEDOT:PSS), have been used as electrodes.

AgNWs are a metallic nanowire material suitable for solution processing. Various studies have shown that AgNWs are the most desirable material as electrodes in flexible electronics due to their high electrical conductivity and flexibility. Nonetheless, their electrical properties largely vary due to high surface roughness, poor interconnection at wire-wire junctions, and a non-uniform random network, which cause poor reliability. Some studies have suggested various methods, including plasmonic welding, embedding method in cross-linkable polymer layer, and transfer method, in an attempt to solve these problems [20–23].

PEDOT is known as a conductive polymer material with one of highest conductivities. However, its modification for processing remains a challenge due to its low solubility. PSS is a representative anionic dispersant that disperses PEDOT into water in the form of PEDOT:PSS and facilitates the solution process. However, its hygroscopic and high acidic characteristics are critical drawbacks for device durability. Furthermore, the insulating PSS reduces the π-π stacking property of PEDOT, causing an electronically inhomogeneous network [24]. To stabilize the network, previous studies have either used polystyrene to which (trifluoromethylsulfonyl)imide (TSFI) was introduced in place of PSS or applied different types of dispersants and dopants such as sulfonated lignin derivatives, methylnaphthalene sulfonate formaldehyde condensate (MNSF), and sulfonated cellulose to achieve remarkable results [25–29]. However, all the aforementioned PEDOT composites, including PEDOT:PSS, are aqueous dispersions and thus are hydrophilic. Therefore, their surface energies do not match with that of hydrophobic PVDF, and dewetting becomes a problem during film formation. Previous studies have attempted to form electrodes through vapor-phase polymerization (VPP) of PEDOT or direct solution-casting polymerization (SCP) to solve the dewetting problem, and these attempts resulted in desirable features [17,30]. Foulger et al. and Im et al. investigated one-dimensional (1D) structures, such as nanofibers and nanowires. Several studies investigated materials featuring a 1D structure using hard templates, such as anodized alumina membrane (AAO) or zeolite, or soft templates, such as SDS or sodium bis(2-ethylhexyl) sulfosuccinate (AOT) [31,32].

In this study, hydrophobic 1D-type PEDOT derivatives, poly(2-butyl-2,3-dihydrothieno[3,4-b][1,4]dioxine:dodecyl sulfate (PEDOT-C_4:DS), and poly(2-hexyl-2,3-dihydrothieno[3,4-b][1,4]dioxine:dodecyl sulfate (PEDOT-C_6:DS) were synthesized by oxidative polymerization using SDS as an anionic surfactant and dopant. These materials were used as electrodes for PVDF-based piezoelectric nanogenerators (PNGs) with a sandwich type structure (electrode/PVDF/electrode).

Hydrophobic PEDOT-C_4:DS and PEDOT-C_6:DS demonstrated similar surface properties to PVDF, which facilitated the fully uniform film formation due to excellent surface matching. Peeling force of PEDOT-C_4:DS and PEDOT-C_6:DS is stronger than the one of PEDOT:PSS-CNT composite. PNG-2 with PEDOT-C_4:DS as electrodes showed the best output performance due to its high conductive morphology, the highest electrical conductivity of PEDOT-C_4:DS (50.0 S cm^{-1}), the highly ordered lamellar structure and dielectric constant (6.74). Also, PNG-3 with PEDOT-C_6:DS as electrodes showed a similar output performance due to its relatively high electrical homogeneity, dielectric constant (3.69), and Young's modulus (50.49 MPa) even though PEDOT-C_6:DS demonstrated an low electrical conductivity (2.7 cm^{-1}). The output voltages PNG-2 and PNG-3 after 25,000 stretching cycles were maintained 97.4% and 94.8% compared to the initial values. It is more stable than the one of PNG-1 (87.6%). Moreover, the charging performance of PNG-2 (3.02 V) and PNG-3 (2.04 V) were better than the one of PNG-1 (1.82 V).

2. Experiments

2.1. Materials

We purchased 3,4-dimethoxythiophene (97%), 1,2-hexanediol (98%), 1,2-octanediol (98%), p-toluenesulfonic acid monohydrate (ACS reagent, ≥ 98.5%), SDS (ReagentPlus®, ≥ 98.5%), iron (III) chloride (reagent grade, 97%), and toluene (anhydrous, 99.8%) from Sigma-Aldrich, and water (HPLC grade) from Fisher Scientific Korea, Ltd. The materials were used without further purification. Pristine PVDF films and PEDOT:PSS-CNT composite-coated PVDF films were purchased from Fils Co., Ltd. The thickness of PVDF was 80 μm.

2.2. Synthesis of monomers

2.2.1. 2-Butyl-2,3-dihydrothieno[3,4-b][1,4]dioxine (2a, EDOT-C_4)

3,4-Dimethoxythiophene (1) (5.0 g, 34.68 mmol), 1,2-hexandiol (4.51 g, 38.14 mmol) and p-toluenesulfonic acid monohydrate (99 mg, 0.52 mmol) were dissolved into toluene (48 ml), and the mixture was stirred for 30 h at 95 °C. The mixture was cooled at room temperature, and the solvent was removed. The product was then washed with a 5% NaOH solution and then with water. The raw material was extracted using chloroform ($CHCl_3$), and the organic layer was dried with sodium sulfate (Na_2SO_4) and filtered. The filtered solution was evaporated. The resulting crude product was purified through column chromatography using silica gel, with hexane as the eluent. Yield: 4.2 g (61.0%) ^{1}H NMR (400 MHz, $CDCl_3$): δ (ppm) 6.3 (s, 2H), 4.16–4.07 (m, 2H), 3.89–3.84 (dd, 1H), 1.73–1.35 (m, 6H), 0.95–0.91 (t, 3H)

2.2.2. 2-Hexyl-2,3-dihydrothieno[3,4-b][1,4]dioxine (2b, EDOT-C_6)

EDOT-C_6 was synthesized with the same method as (1), but 1,2-octanediol (5.6 g, 38.14 mmol) was used in place of 1,2-hexandiol. Yield: 3.9 g (49.7%) ^{1}H NMR(400 MHz, $CDCl_3$): δ (ppm) 6.3 (s, 2H), 4.16–4.07 (m, 2H), 3.89–3.84 (dd, 1H), 1.73–1.30 (m, 10H), 0.91–0.87 (t, 3H)

2.3. Synthesis of PEDOT-C_4:DS and PEDOT-C_6:DS

Poly(2-butyl-2,3-dihydrothieno[3,4-b][1,4]dioxine:dodecyl sulfate (PEDOT-C_4:DS):

An aqueous iron(III) chloride solution (1.16 M) was slowly added to a SDS solution (0.347 M). The solution was then stirred for 1 h at 50 °C, and 2-butyl-2,3-dihydrothieno[3,4-b][1,4]dioxine (0.69 g, 3.5 mmol) was slowly added. The new solution was stirred for 48 h at the same temperature and was poured into MeOH. The obtained powder was filtered and washed with water and MeOH. The final powders were vacuum-dried at 60 °C for 24 h, and the yield was 80.9%.

Poly(2-hexyl-2,3-dihydrothieno[3,4-b][1,4]dioxine:dodecyl sulfate (PEDOT-C_6:DS):

PEDOT-C_6:DS was synthesized with the same method used for

PEDOT-C_4:DS. 2-Hexyl-2,3-dihydrothieno[3,4-b][1,4]dioxine (0.79 g, 3.5 mmol) was used in place of 2-butyl-2,3-dihydrothieno[3,4-b][1,4] dioxine, and the yield was 45.5%.

2.4. Preparation of PEDOT-C_x:DS solution and device fabrication

First, 0.7 wt% and 1.0 wt% solutions of PEDOT-C_4:DS and PEDOT-C_6:DS were prepared using N,N-dimethylformamide(DMF) and 1,2-dichlorobenzene(ODCB), respectively. The samples were filtered using a 5.0 μm nylon filter prior to use.

Fig. S1 represents the PNG fabrication process performed in this study. One side of the PVDF film (35 × 35 mm^2) was spin-coated with the PEDOT-C_4:DS solution at 1000 rpm for 30 s. The film was then dried at 60 °C for 15 min to form a thin-film electrode layer. The same process was repeated on the other side, and sandwich-structured (electrode/PVDF/electrode) PNG-2 was fabricated. Finally, the film was cut to 25 × 15 mm^2 for use. PNG-3 was produced with the same method using PEDOT-C_6:DS. A PEDOT:PSS-CNT composite-coated PVDF film purchased from Fils Co., Ltd. was used as a reference PNG-1 and was cut to the same size for use.

2.5. Characterization

XPS spectra were measured using a K-Alpha + (Thermo Fisher Scientific Co., USA) with an Al Kα source (1486.6 eV). The XPS spectra were calibrated in reference to the C 1 s peak (284.5 eV). FE-SEM images of the PEDOT-C_4:DS and PEDOT-C_6:DS powders and these thin-film surfaces formed on the PVDF film were observed using a Nova Nano SEM 200 (FEI Company, USA) under a 5.0 kV accelerating voltage. TEM images of the PEDOT-C_4:DS and PEDOT-C_6:DS powders were observed using JEM-1010 (JEOL, Japan). The contact angles of deionized (DI) water on the sample films were measured using a DSA 100 (KRŰSS, Germany). The 180° peel-off test for adhesion properties was carried out using EZ-SX (SHIMADZU, Japan). The cross-sectional images of PNG-(0 − 3) were observed, and the thickness of the PEDOT-C_4:DS and PEDOT-C_6:DS thin films were measured using a Helios NanoLab 600 (FEI Company, USA). The morphologies and current maps of the samples were observed using a XE-100 (Park Systems, Republic of Korea) with a Cdt-contr cantilever and were measured in an area of 3 × 3 μm^2 in contact mode. XRD patterns were measured to analyze the crystalline phase of PVDF, PEDOT-C_4:DS and PEDOT-C_6:DS using a SmartLab (Rigaku, Japan). The crystalline structures of PEDOT-C_4:DS and PEDOT-C_6:DS thin films were characterized with two-dimensional grazing incidence wide angle X-ray scattering (2D-GIWAXS) at the 3 C beamline of the Pohang accelerator laboratory (PAL). An ATR-FTIR spectrum was measured to identify the structure of PVDF using a FT/IR 4100 (JASCO, Japan). The surface resistance of each sample was measured using a ST-4 work surface tester (SIMCO Co., Japan), and the measured size was 5 × 5 cm^2. One end of the produced PNGs was fixed to the homemade tester. The stretch and release were repeatedly measured with the other side in the uniaxial direction. The measurement condition was a 1.0 Hz frequency with a 0.2 mm displacement. Output voltages and currents were measured using a DMM7510 graphical sampling multimeter (Keithley, USA). The dielectric constant of each sample was measured using a LCR meter, E4980A (Agilent, USA). Stress-strain curves of samples were observed using a micro-fatigue tester, E3000LT (Instron, USA).

3. Results and discussion

Fig. 1 shows a schematic illustration of the synthetic process (a~g) and molecular structures (h) of PEDOT-C_4:DS and PEDOT-C_6:DS. The synthetic route to the monomers and polymers is shown in Scheme S1. First, an SDS (Fig. 1a) concentration greater than the critical micelle concentration (CMC) was added to the aqueous solution (300 mM). SDS, which forms a primary micelle structure (Fig. 1b), gradually formed a spherical, ellipsoidal structure (Fig. 1c and d), and finally a cylindrical structure (Fig. 1e). The solution was colorless when the cylindrical structure formed, which corresponded to the result found by S. H. Foulger et al. [33]. After the iron chloride (III) ($FeCl_3$) solution was added as an oxidant, the color of the solution changed to ivory. Then, the solution was gradually heated and stirred at 50 °C for 1 h. The color of the solution gradually turned orange resulting from the formation of a more solid cylindrical structure (Fig. 1e) due to the increased ionic strength and electrostatic interaction of iron cations and DS anions. Monomers, 2-butyl-2,3-dihydrothieno[3,4-b][1,4]dioxine

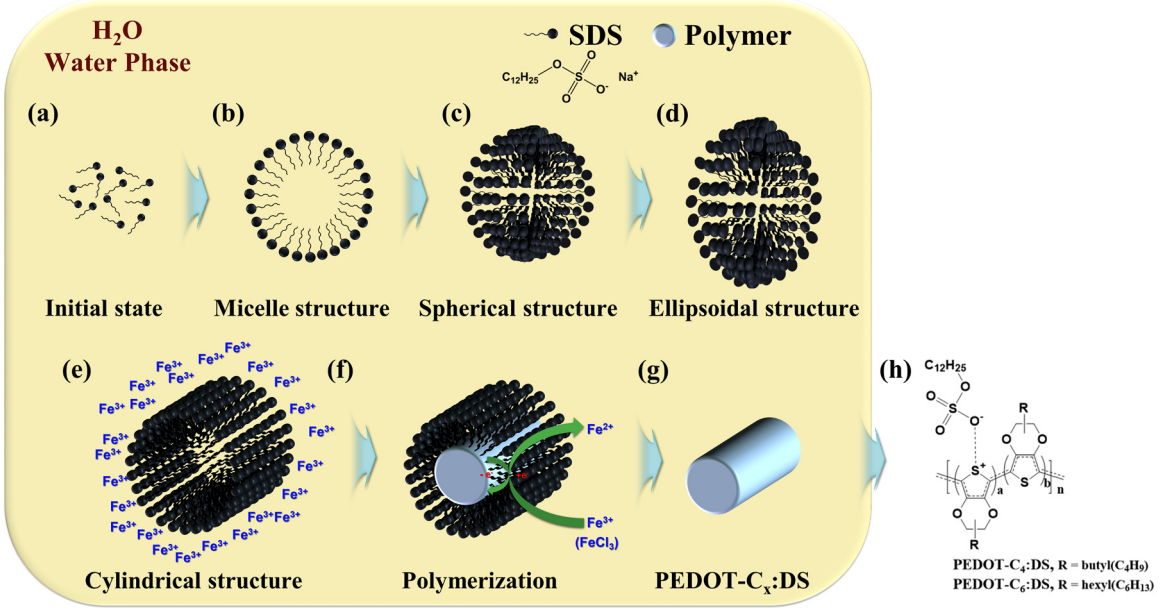

Fig. 1. Schematic illustration of the synthetic process in aqueous SDS micelle solution; initial state of SDS (a), the formation of a primary micelle structure of SDS in critical micelle concentration (CMC) (b), gradual changes of SDS from a spherical structure (c) to an ellipsoidal structure (d), the final formation of SDS in a cylindrical structure. After adding $FeCl_3$ oxidant, the cylindrical SDS is surrounded by iron(III) cations to be more cylindrical structure (e), the polymerization of PEDOT-C_4 and PEDOT-C_6 inside of the SDS structure (f), the obtained PEDOT-C_x:DS (g) and molecular structures of PEDOT-C_x:DS (x = 4 or 6) (h).

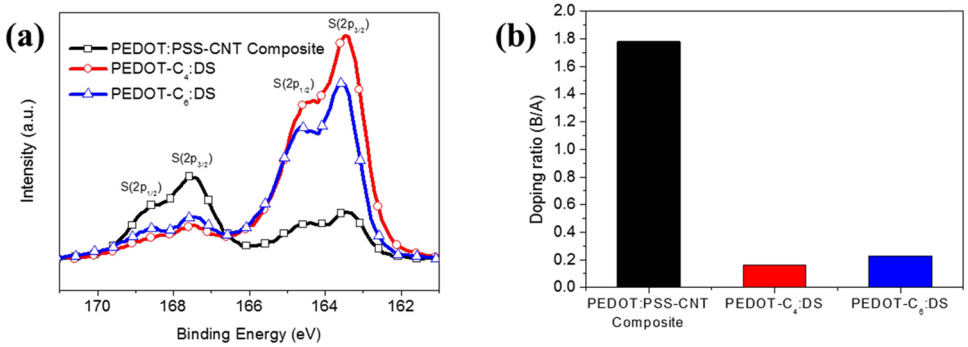

Fig. 2. S(2p) XPS spectra (a) and doping ratio (B/A) (b) of PEDOT:PSS-CNT composite, PEDOT-C_4:DS, and PEDOT-C_6:DS (A: PEDOT derivatives, B: Dopants).

(EDOT-C_4) and 2-hexyl-2,3-dihydrothieno[3,4-b][1,4]dioxine (EDOT-C_6), were then added to the solution. The added monomers moved to the inside of the hydrophobic cylindrical micelle and were synthesized by oxidative polymerization, as shown in Fig. 1(f) [32,33]. The obtained polymeric materials have a main chain of monomers in which the butyl and hexyl groups were introduced to EDOT as side chains, as shown in Scheme S1. The obtained products were filtered and washed with deionized (DI) water and MeOH, and the final products (Fig. 1g) were dried in the vacuum state at 60 °C for 24 h, showing yields of 80.9% and 45.5%, respectively.

Fig. 2 shows the X-ray photoelectron spectroscopy (XPS) S(2p) spectra (Fig. 2a) and doping ratio (B/A, Fig. 2b) of anionic dopants (B), such as PSS and DS, to PEDOT derivatives (A). In Fig. 2(a), the S($2p_{1/2}$) and S($2p_{3/2}$) peaks corresponding to the thiophene of PEDOT were ~164.7 eV and ~163.5 eV, respectively. The S($2p_{1/2}$) and S($2p_{3/2}$) peaks of the sulfonated groups of the PSS anion and DS anion were ~168.7 eV and ~167.5 eV [34–37]. As in the S($2p_{3/2}$) peak area ratio in Fig. 2(b), the reference PEDOT:PSS-CNT composite showed the highest PSS anion to PEDOT ratio of 1.78. In contrast, the DS anion to PEDOT-C_4 and PEDOT-C_6 ratios of PEDOT-C_4:DS and PEDOT-C_6:DS were 0.16 and 0.23, respectively. The doping ratios of the dopant (DS anion) to the PEDOT derivatives synthesized in this study were approximately 9% and 14.6%, which are remarkably lower than those of the reference, and these values correspond well to the results of previous studies, which have shown that PEDOT-C_4:DS and PEDOT-C_6:DS are affected by dopants to a lesser degree, while they effectively contribute to the formation of a conductive network with improved conductivity [38–40]. The results are shown in Table 1.

Fig. 3(a–d) shows the field-emission scanning electron microscopy (FE-SEM) (Fig. 3a and c) and transmission electron microscopy (TEM) (Fig. 3b and d) images of PEDOT-C_4:DS and PEDOT-C_6:DS. These two polymers had a similar surface morphology, as shown in the FE-SEM images, and had a bulk state one-dimension structure. The TEM images show a nanofiber state one-dimensional structure from which polymer composites were separated, which is similar to the result of PEDOT-NF reported by Im et al. [32]. The diameters of these two PEDOT derivative (PEDOT-C_4:DS and PEDOT-C_6:DS) nanofibers ranged from 40 to 80 nm on average.

Fig. 3(e–h) shows the contact angle images of DI water dropped on the film surface. PVDF (e) was measured at a contact angle of 83.4°, as shown in Table 1. The contact angles of the PEDOT:PSS-CNT composite (f), and the PEDOT-C_4:DS (g) and PEDOT-C_6:DS (h) coated on PVDF were 56.6°, 76.6°, and 87.7°, respectively. PEDOT derivatives demonstrated hydrophobicity even when doped by DS anions, unlike the PEDOT:PSS-CNT composite, and the hydrophobicity resulted from the hydrophilic sulfate head group (SO^{3-}) of the DS anion fixed to the PEDOT derivatives, and the hydrophobic dodecyl tail group in the opposite direction. The surface energy was calculated using the Owens, Wendt, Rabel and Kaelble (OWRK) method [41]. The surface energy of hydrophobic PVDF was calculated to be 22.94 mN m^{-1}. The surface energies of the PEDOT:PSS-CNT composite, PEDOT-C_4:DS, and PEDOT-C_6:DS films were 44.37 mN m^{-1}, 28.0 mN m^{-1}, and 19.97 mN m^{-1}, respectively. When the side chain lengths of the EDOT monomers became longer, changing from butyl(C_4) to hexyl(C_6), the surface energy decreased, and EDOT demonstrated higher hydrophobicity [35,42]. The PEDOT:PSS-CNT composite exhibited a large surface energy gap ($\Delta SE = 21.43$ mN m^{-1}) mismatch with PVDF due to its relative hydrophilicity, which corresponds with the results seen in the XPS data (Fig. 2). In other words, the surface properties of the introduced organic electrode layers were determined by the doping properties of the PSS anion and DS anion dopants. These results were achieved because PEDOT-C_4:DS and PEDOT-C_6:DS demonstrated similar hydrophobicity to the piezoelectric active material PVDF, which facilitated the formation of a fully uniform film due to excellent surface energy matching [43–45]. In order to investigate the adhesion characteristics of the organic electrode layers on PVDF, 180° peel-off test with scotch tape was performed using a tensile tester at 100 mm/min as shown in Fig. 3(i). The peeling force of PEDOT:PSS-CNT composite, PEDOT-C_4:DS and PEDOT-C_6:DS on PVDF were 3.76 N, 4.19 N and 4.24 N respectively in Fig. 3(m). The peeling force of PEDOT-C_4:DS and PEDOT-C_6:DS is stronger than the one of PEDOT:PSS-CNT composite, which means hydrophobic PEDOT derivatives are adhered relatively stronger than

Table 1
Surface and electrical properties of all materials.

	Doping ratio[a]	Contact angle [°]	Surface Energy [mN m^{-1}]	Thickness [nm]	Sheet Resistance [kΩ/sq]	Conductivity [S cm^{-1}]
PVDF	–	83.4	22.94	–	–	–
PEDOT:PSS[b]	–	–	–	105[c]	79.0	1.2
PEDOT:PSS-CNT composite	1.78	56.6	44.37	40	13.0	19.2
PEDOT-C_4:DS	0.16	76.6	28.0	100	2.0	50.0
PEDOT-C_6:DS	0.23	87.7	19.97	60	63.0	2.7

[a] The ratio of dopants to PEDOT derivatives.
[b] PEDOT:PSS (Clevios PH-1000, Heraeus) was spin-coated on glass at 1500 rpm for 30 s and annealed at 120 °C for 15 min.
[c] Measured by alpha step 500 surface profiler (KLA-Tencor).

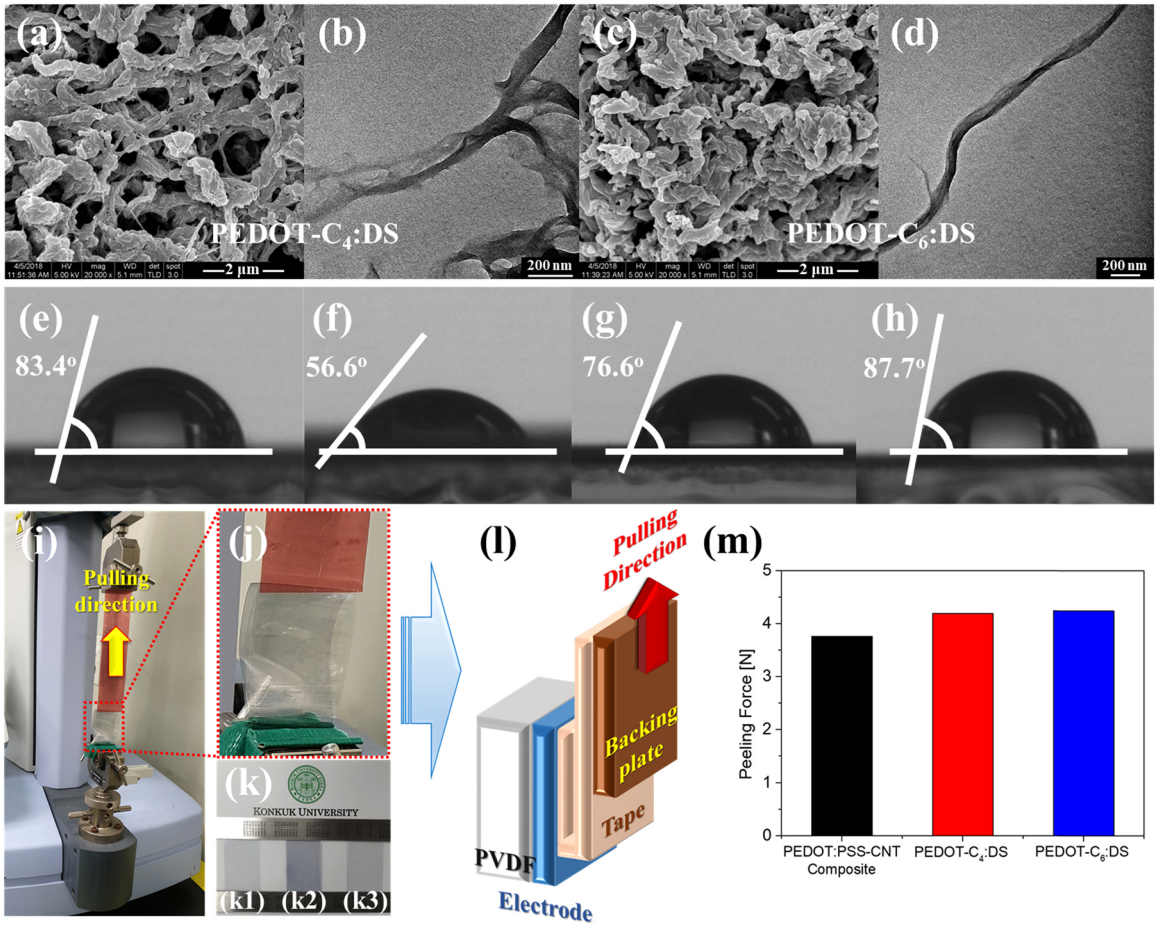

Fig. 3. The FE-SEM (a and c) and TEM (b and d) images of PEDOT-C_4:DS and PEDOT-C_6:DS. Contact angle images of DI water droplets on PVDF (e), PEDOT:PSS-CNT composite (f), PEDOT-C_4:DS (g), PEDOT-C_6:DS (h) films. A photograph of peel-off tester (i), an enlarged photograph of a testing sample (j), and samples (k); PEDOT:PSS-CNT composite (k1), PEDOT-C_4:DS (k2), and PEDOT-C_6:DS (k3). Schematic illustration of 180° peel-off test of organic electrode layers coated on PVDF (l). Peeling force of each sample at 100 mm/min (m).

the hydrophilic PEDOT:PSS-CNT composite on PVDF [46].

Fig. S2(a–c) is the cross-sectional images of the organic electrodes coated on PVDF measured with a focused ion beam (FIB). PEDOT:PSS-CNT composite (a), PEDOT-C_4:DS (b), and PEDOT-C_6:DS (c) layers were ca. 40 nm, 100 nm, and 60 nm, respectively, and their sheet resistances were 13.0, 2.0, and 63.0 kΩ sq^{-1}, respectively. PEDOT-C_4:DS demonstrated an electrical conductivity (σ = 50.0 S cm^{-1}) approximately 2.6 times greater than that of the PEDOT:PSS-CNT composite (σ = 19.2 S cm^{-1}) and approximately 18.5 times higher than that of PEDOT-C_6:DS (σ = 2.7 S cm^{-1}). PH-1000 spin-coated on glass was used as a comparison to pristine PEDOT:PSS, and its thickness was 105 nm, its sheet resistance was 79.0 kΩ sq^{-1}, and its conductivity was 1.2 S cm^{-1}. The synthesized PEDOT-C_4:DS and PEDOT-C_6:DS demonstrated conductivities of 41.7 and 2.25 times higher than that of pristine PEDOT:PSS, respectively. The results are shown in Table 1.

Fig. 4 demonstrates FE-SEM images (a1, b1, c1) of the surface morphologies of the PEDOT:PSS-CNT composite (a), PEDOT-C_4:DS (b) and PEDOT-C_6:DS (c) coated on PVDF; and topographic images (a2, b2, c2) and conductive atomic force microscopy images (a3, b3, c3) measured with C-AFM to analyze the homogeneity of the electrical conductivity. C-AFM was operated at 0.5 V with forward bias in contact mode, and topographic images and current map images were simultaneously obtained. The schematic diagram of C-AFM is in Fig. S3.

As shown in Fig. 4(a1 and a2), the PEDOT:PSS-CNT composite generally formed a porous network, and some aggregates were locally observed. However, the root-mean-square (RMS) roughness was 3.527 nm, and the morphology was smooth. As shown in Fig. 4(b1 and b2), PEDOT-C_4:DS formed a clear nanofibrillar network with a relatively higher RMS roughness (5.936 nm) [47,48]. As shown in Fig. 4(c1 and c2), PEDOT-C_6:DS, which consists of EDOT with a hexyl alkyl chain of 6 carbons, had a smoother morphology than did PEDOT-C_4:DS and a lower RMS roughness of 3.687 nm. In brief, PEDOT-C_6:DS features a relatively greater solubility to solvents than did PEDOT-C_4:DS.

As shown in Fig. 4(a3), the current map image of the PEDOT:PSS-CNT composite shows the existence of a high conductive area (bright part) with a major distribution of low conductive areas (dark part), which cause surface charge losses and reduce the flow of charge to the external circuit. In turn, poorly distributed conductive network results in a low piezoelectric output signal. In contrast, the current map image of PEDOT-C_4:DS (Fig. 4(b3)) shows that the high conductive area has a greater distribution and is more continuous along the nanofibrillar network. The current of the bright areas was the highest, corresponding to the lowest doping ratio of DS anion and a high conductivity. The current map image (Fig. 4(c3)) of PEDOT-C_6:DS shows the lowest RMS current (39.258 nA), and the most uniform electrical distribution [28].

Fig. 5(a1) shows X-ray diffraction (XRD) patterns of the thin films. In the case of the PVDF film (Fig. 5(a1–1)) used in this study, diffraction peaks were observed at 2Θ = 20.6° (110/200), 36.6° (020/101), and 56.9° (221). As shown in Fig. S4, the attenuated total reflectance Fourier-transform infrared spectroscopy (ATR-FTIR) spectrum peaks of PVDF were observed at 1430, 1276, and 839 cm^{-1}, forming the β-phase [49,50]. The diffraction peaks of the three polymeric materials were not clearly visible due to PVDF, and thus, the spectra were enlarged from

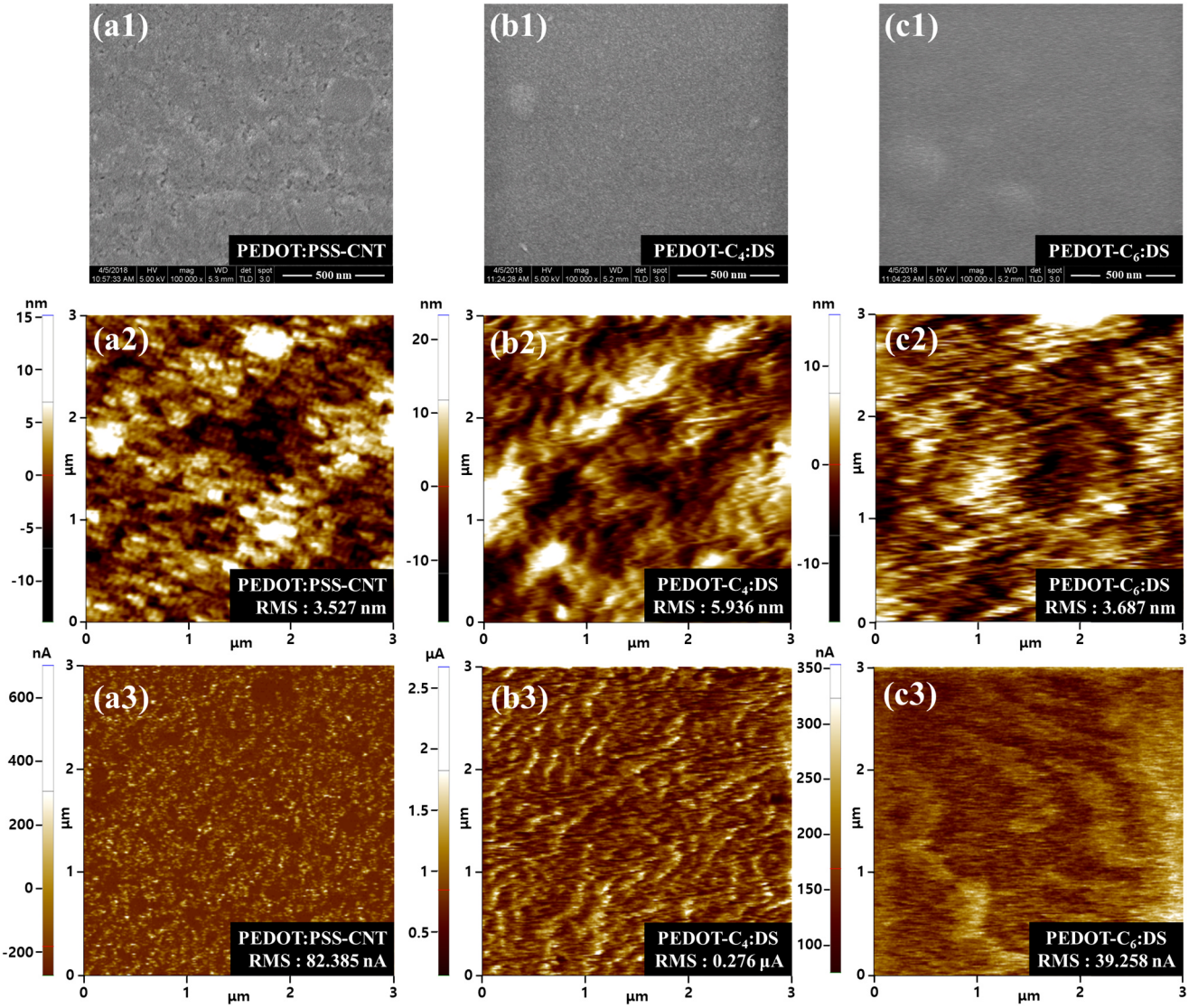

Fig. 4. The FE-SEM images (a1, b1, c1) about surface morphologies and conductive AFM images of films coated on PVDF; topographical (a2, b2, c2) and current map (a3, b3, c3) images of PEDOT:PSS-CNT composite, PEDOT-C_4:DS and PEDOT-C_6:DS.

$2\Theta = 3^\circ$ to $2\Theta = 12^\circ$, as shown in Fig. 5(a2). The PEDOT:PSS-CNT composite was amorphous, demonstrating no peaks. However, diffraction peaks of PEDOT-C_4:DS and PEDOT-C_6:DS exhibited (100) diffraction peaks at $2\Theta = 4.38^\circ$ and 3.22°, respectively, forming a lamellar orientation. The lamellar distance was 20.16 Å and 27.46 Å, respectively. However, the intensities of PEDOT-C_x:DS film peaks are too low to analyze due to the strong intensities of PVDF. For a more accurate analysis, PEDOT-C_4:DS and PEDOT-C_6:DS thin films were coated on Si substrates. The measured GIWAXS images and the corresponding lincut profiles are shown in Fig. 5(b and c). PEDOT-C_4:DS showed the strong (100) diffraction peak at $q_z = 0.36\ \text{Å}^{-1}$, the weak (200) diffraction peak at $q_z = 0.75\ \text{Å}^{-1}$ and the weak (010) diffraction peak at $q_z = 1.60\ \text{Å}^{-1}$ in the out-of-plane direction, and the strong (010) diffraction peak at $q_{xy} = 1.67\ \text{Å}^{-1}$ in the in-plane direction. On the other hand, PEDOT-C_6:DS showed the strong (100) diffraction peak at $q_z = 0.24\ \text{Å}^{-1}$ and the weak (010) diffraction peak at $q_z = 1.60\ \text{Å}^{-1}$ in the out-of-plane direction, but the relatively weaker (010) diffraction peak at $q_{xy} = 1.47\ \text{Å}^{-1}$ than the (100) diffraction peak at $q_{xy} = 0.28\ \text{Å}^{-1}$ in the in-plane direction. Therefore, PEDOT-C_6:DS formed bimodal orientation consisting of edge-on and face-on structures. The distance of chain-to-chain (lamellar stacking) was 17.31 Å and 26.07 Å, respectively [51,52]. PEDOT-C_4:DS with a side chain of a 4-carbon butyl group is shorter in length than PEDOT-C_6:DS with a 6-carbon hexyl group, thus forming a dense polymer chain, which dramatically improves the crystallinity and forms a more suitable ordered lamellar structure. According to the results, PEDOT-C_4:DS formed the highly ordered edge-on orientation, which is more efficient orientation for charge transport in one way. PEDOT-C_6:DS formed the edge-on orientation mainly and face-on orientation slightly. The schematic diagram of PEDOT-C_4:DS and PEDOT-C_6:DS structures is in Fig. S5.

Fig. 6(a–c) demonstrates the process of power generation from the PNGs produced in this study. Their structure ($25 \times 15\ \text{mm}^2$) consists of a sandwich-type electrode/PVDF/electrode. The PNGs were named PNG-1(PEDOT:PSS-CNT composite), PNG-2(PEDOT-C_4:DS), and PNG-3(PEDOT-C_6:DS) according to the materials used as electrodes. For the measurement, one end was fixed to the tester, and the stretch and release of the other end was measured in the uniaxial direction at a 1.0 Hz frequency, $0.4\ \text{mm s}^{-1}$ drive speed and 0.8% strain (0.2 mm displacement). The upper and bottom electrodes formed on PVDF were connected to the multimeter to measure the output signals (voltages and currents). As shown in Fig. 6(a), the output signal was 0 because there was no change in the dipole moment during the initial state without any externally applied force. As in Fig. 6(b), when β-phase PVDF is strained along the uniaxial direction, the piezoelectric potential changes due to a

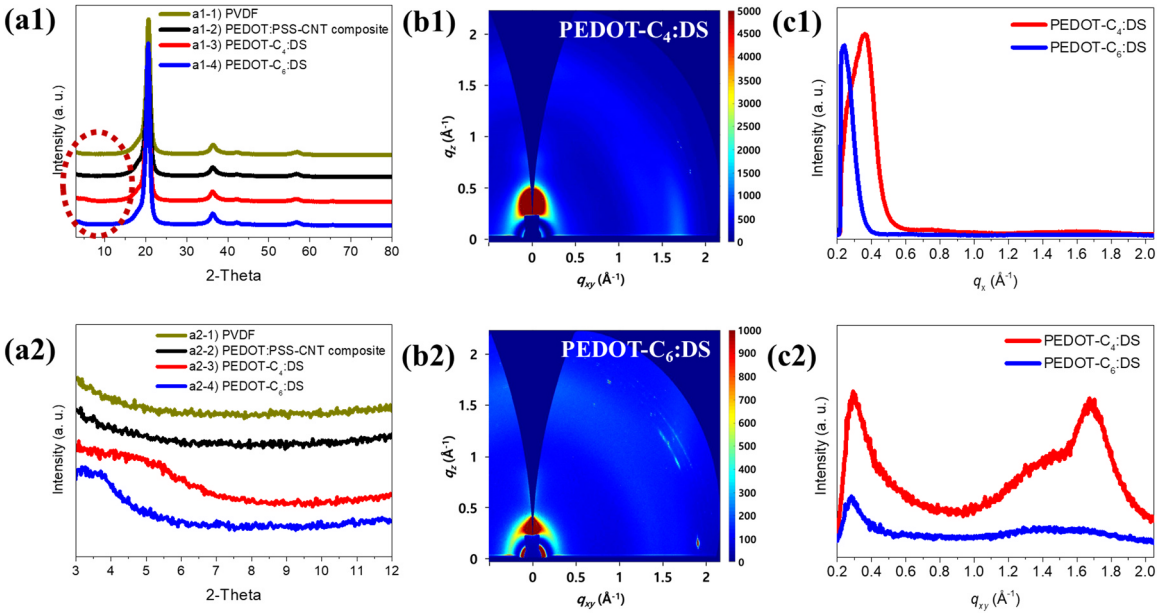

Fig. 5. XRD spectra of PVDF, PEDOT:PSS-CNT composite, PEDOT-C_4:DS and PEDOT-C_6:DS on PVDF (a); from 3° to 80° (a1), from 3° to 12° in red-dot circle (a2). 2D-GIWAX images of PEDOT-C_x:DS films on Si substrates (b); PEDOT-C_4:DS (b1) and PEDOT-C_6:DS (b2). Corresponding line cut profiles of the 2D-GIWAX images (c); out-of-plane linecuts (c1) and in-plane linecuts (c2). (For interpretation of the references to color in this figure legend, the reader is referred to the web version of this article.)

decrease in total spontaneous polarization. The holes in the upper electrode drift to the lower electrode due to the weak negative piezoelectric potential. Additionally, electrons in the lower electrode drift to and accumulate in the upper electrode due to the weak positive piezoelectric potential, resulting in a positive output signal. As in Fig. 6(c), the generated potentials disappear when an external force is released, and a negative output signal occurs as the accumulated charges return to the initial state for balance [53–55].

Fig. 6(d and e) show the piezoelectric output voltages and currents of the PNG-(1 − 3), respectively. The results are shown in Table 2. The mean maximum peaks of output voltages (V_{avg}, V) of each device, as shown in Fig. 6(d), were V_{avg}(PNG-1) = 1.25 V, V_{avg}(PNG-2) = 1.54 V,

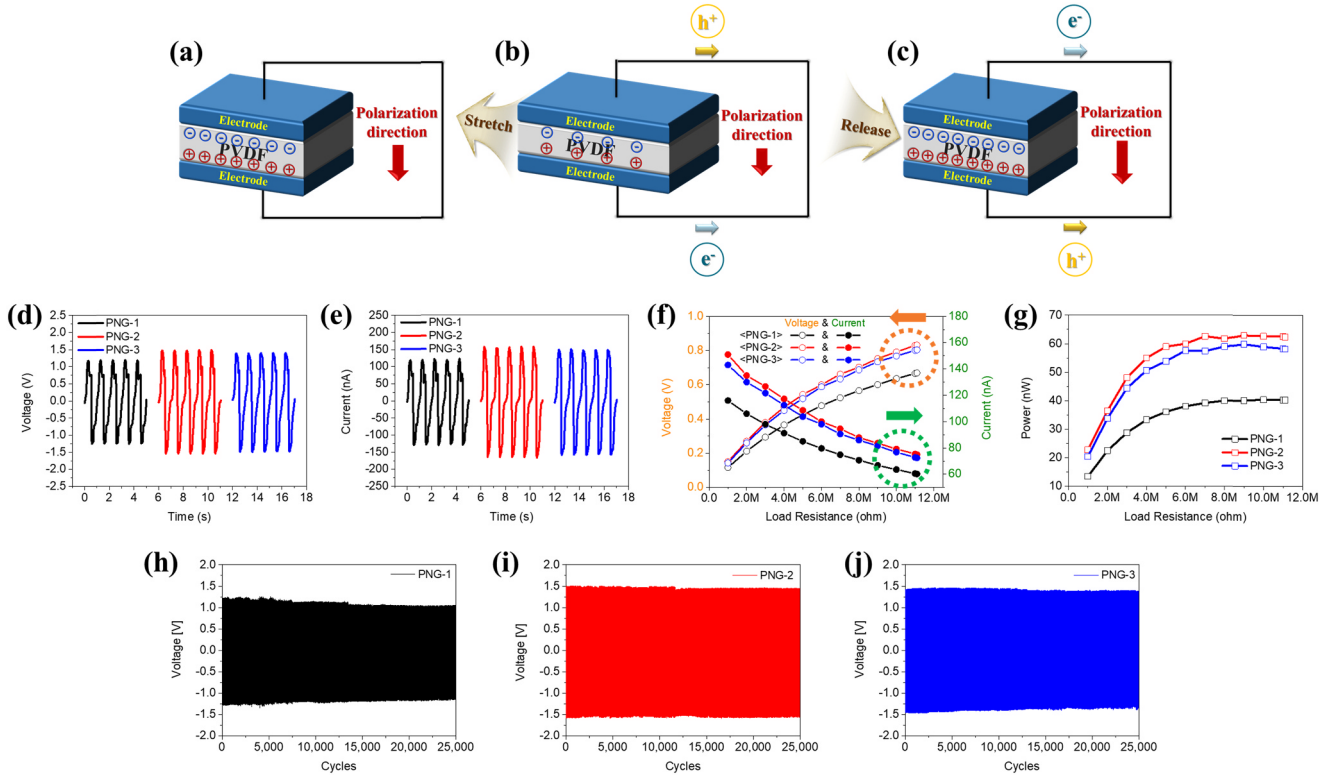

Fig. 6. Schematic illustration of power generation; no strain (a), stretching (b) and releasing (c). Piezoelectric output signals of the PNG-(1 − 3); output voltages (d) and output currents (e). The max output voltages and currents across the different load resistance (f) and the output power depending on the load resistance (g). The output voltages of PNG-1 (h), PNG-2 (i), and PNG-3 (j) upon 25,000 cycles for a stability test.

Table 2
The average of measured maximum output performance of PNGs.

	Voltage [V]	Current [nA]	Load Resistance [MΩ]	Power [nW]
PNG − 1	1.25	128.5	10	41.0
PNG − 2	1.54	166.0	9	63.0
PNG − 3	1.49	159.0	9	59.9

and V_{avg}(PNG-3) = 1.49 V. PNG-2 and PNG-3 demonstrated output voltages improved by 23.2% and 19.2%, respectively, compared to that of PNG-1. As in Fig. 6(e), the measured mean maximum peaks of the output currents (I_{avg}, nA) of each device were I_{avg}(PNG-1) = 128.5 nA, I_{avg}(PNG-2) = 166.0 nA, and I_{avg}(PNG-3) = 159.0 nA, respectively. PNG-2 and PNG-3 demonstrated output currents improved by 27.7% and 22.3% compared to that of PNG-1. Fig. 6(f and g) show the results of the output voltages, currents, and power according to the load resistance when each of the PNGs was connected to the resistor decade box. The max output power (nW) with optimized resistance was calculated using the equation below.

$$W = V \times I = V^2/R \quad (1)$$

As shown in Table 2, PNG-1 was optimized at 10 MΩ, and PNG-2 and PNG-3 were optimized at 9 MΩ. The maximum output power was 41.0 nW, 63.0 nW, and 59.9 nW for PNG-(1 − 3), respectively. PNG-2 and PNG-3 demonstrated a performance improved by 53.7% and 46.1% compared to that of PNG-1 due to the well-matched adhesion property between the layers. Because hydrophobic PEDOT-C_4:DS and PEDOT-C_6:DS have surface energies similar to that of PVDF, charge transfer between PVDF and PEDOT-C_x:DS is better than the one between PVDF and PEDOT:PSS-CNT composite due to stronger interaction. PEDOT:PSS-CNT composite is hydrophilic, which cause a poor interfacial contact with PVDF resulting lower output performance. PNG-2 with PEDOT-C_4:DS demonstrated the best piezoelectric output signals; this result corresponds well with the similar surface energy between two materials, the current map results shown in Fig. 4(b3), the highly ordered edge-on orientation shown in Fig. 5 and the properties of conductivity shown in Table 1.

Fig. S6 shows the electrostatic potential and net dipole moments of PEDOT:PSS, PEDOT-C_4:DS and PEDOT-C_6:DS. Density functional theory (DFT) calculation with the B3LYP/6–31G(d) was used for those of molecular simulations. For simple calculations, trimers of PEDOT, PEDOT-C_4 and PEDOT-C_6 were used as conductive structure, tri-EDOT, tri-EDOT-C_4 and tri-EDOT-C_6, respectively. Also, p-toluenesulfonate(p-TS) and ethylsulfonate(ES) as dopants instead of PSS and DS were used. Therefore, tri-EDOT:p-TS, tri-EDOT-C_4:ES and tri-EDOT-C_6:ES were calculated.

tri-EDOT:p-TS represents a partial positive charge on tri-EDOT and a partial negative charge on p-TS. tri-EDOT-C_4:ES and tri-EDOT-C_6:ES represent partial positive charges on tri-EDOT-C_4 and tri-EDOT-C_6 and partial negative charges on ES. As shown in Fig. S2(d∼f), net dipole moments of tri-EDOT:p-TS, tri-EDOT-C_4:ES and tri-EDOT-C_6:ES are 10.23 Debye, 16.17 Debye, and 14.49 Debye, respectively.

Fig. S7 shows the dielectric constants of PVDF films with all the organic electrodes. The dielectric constants of PVDF films with PEDOT:PSS-CNT composite, PEDOT-C_4:DS and PEDOT-C_6:DS are 1.3, 6.74 and 3.69 at 1 kHz, respectively. PVDF films with hydrophobic PEDOT-C_4:DS and PEDOT-C_6:DS nanofiber films show higher values about 5.2 and 2.8 times than the one with hydrophilic PEDOT:PSS-CNT composite, which give rise to accumulation of more charge carriers at the interface. Also, the net dipole moments of PEDOT-C_4:DS trimer and PEDOT-C_6:DS trimer are larger than the one of PEDOT:PSS trimer, which is efficient for charge transport as shown in Fig. S6 [56–58].

Young's modulus(E) is a factor for electrochemical coupling factor ($k = d[E/\varepsilon]^{1/2}$), which converts mechanical energy to electrical energy, where d is piezoelectric coefficient, E is Young's modulus, and ε is dielectric constant. Fig. S8 shows stress-strain curve of PVDF films with all the organic electrodes. The Young's modulus of PVDF films with PEDOT:PSS-CNT, PEDOT-C_4:DS, and PEDOT-C_6:DS are 48.35 MPa, 37.51 MPa, and 50.49 MPa, respectively. PVDF film with PEDOT-C_4:DS showed decreased Young's modulus, which could be negative for output

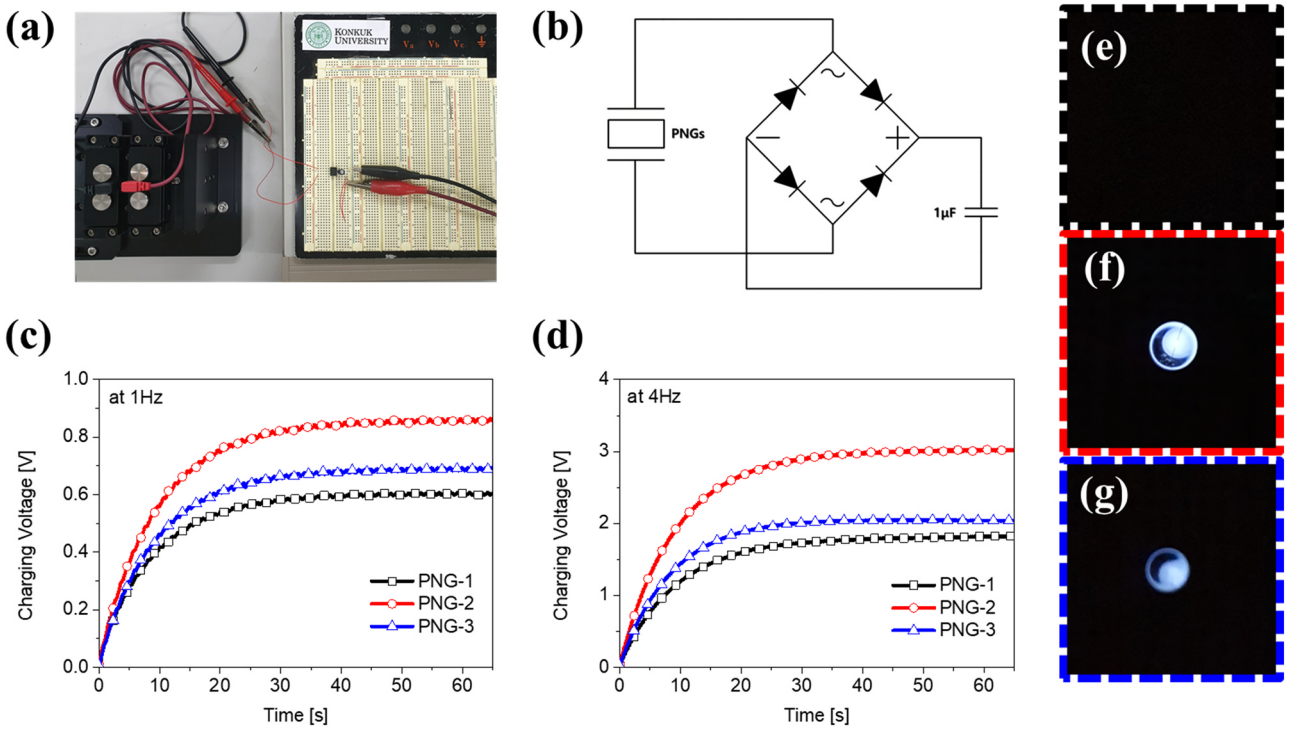

Fig. 7. A Photograph of the energy storage system (a), the charging circuit diagram (b), and the charged voltage curves at 1 Hz (c) and at 4 Hz (d) of 1 μF capacitor. The snapshots of white LEDs driven by PNG-1 (e), PNG-2 (f), and PNG-3 (g).

performance. However, the one with PEDOT-C_6:DS showed enhanced Young's modulus, which is positive for piezoelectric properties [59].

Therefore, PNG-3 with PEDOT-C_6:DS shows piezoelectric output signals higher than those of PNG-1 with PEDOT:PSS-CNT composite, despite the relatively lower conductivity of PEDOT-C_6:DS, which corresponds well with the excellent electrical homogeneity (Fig. 4(c3)), with the surface energy most similar to PVDF and with enhanced dielectric constant and Young's modulus [28].

These results caused relatively higher piezoelectric output signals of PNG-2 & 3 with hydrophobic PEDOT-C_4:DS and PEDOT-C_6:DS even though PEDOT-C_6:DS had relatively high sheet resistance and low conductivity.

Talemi et al. demonstrated that vapor phase polymerized (VPP) PEDOT coated PVDF-based piezoelectric harvester showed high output performance up to 0.55 V under 3mN bending force with PVDF surface plasma treatment as enhancing adhesion property between two polymers. Also, Park et al. demonstrated that a PVDF harvester with PP-PEDOT by solution casting polymerized (SCP) method showed about 1.4 V under 380mN strain force as matching surface energy with PVDF [17,30]. The methods mentioned above are quite good for enhancing output performance of PVDF based PNGs. However, PVDF based PNG with these types of hydrophobic PEDOT derivatives can be fabricated with more simple process and show quite good performance even with small size PNGs.

Also, all of the PNGs were measured output voltages upon 25,000 stretching cycles at the same condition for the stability test as shown in Fig. 6(h–j). PNG-1 maintained the average output voltage of 87.6% compared to the initial value after 25,000 cycles. PNG-2 and PNG-3 maintained 97.4% and 94.8%, respectively. The PVDF based PNGs with hydrophobic PEDOT-C_x:DS electrodes showed better stability, as well.

In Fig. 7, The PNGs were connected to the bridge circuit and the 1 μF capacitor to investigate the charging performance. The test was carried out at 1 Hz (c) and 4 Hz (d) as the same displacement (0.2 mm) applying the stretching force. At 1 Hz, the 1 μF capacitor was charged by PNG-(1 − 3) to 0.61 V, 0.86 V, and 0.70 V in 60 s, respectively. In the case of 4 Hz condition, the capacitor was charged to 1.82 V, 3.02 V, and 2.04 V in 60 s, respectively. The charging voltages are proportional to the output characteristics of PNG-1, PNG-3, and PNG-2 demonstrating high in the order as in Fig. 6 [60]. The brightness of the white LEDs enhanced in the order of PNG-1, PNG-3, and PNG-2 as shown in Fig. 7(e–g). PNG-1 hardly turned on the LED, but PNG-3 slightly turned on the LED and PNG-2 turned on the LED, perfectly.

PNGs that can generate electrical energy directly from mechanical energy are one of the promising ways to resolve power source of self-powered system, such as biomedical sensors, body motion sensors, wearable devices and etc [61–65]. Fig. 8 demonstrates the output voltage performance of PNG-(1 − 3) in self-powered piezoelectric sensor applications. As shown in Fig. 8(a) and Movie S1, PNGs were attached to wrist by finger to measure human heartbeat, and the pulse of the subject was 76 beats per minute on average. The output voltage values of PNG-(1 − 3) are 20 mV, 35 mV, and 30 mV on average, respectively. The results of PNG-2 and PNG-3 are 75% and 50% higher than the one of PNG-1. In addition, PNG-(1 − 3) were fixed tightly to the index finger with a medical tape to measure finger motion states at bending angle of ~30° as shown in Fig. 8(b) and Movie S2. The output voltage values of PNG-(1 − 3) are up to 0.66 V, 0.99 V, and 0.91 V, respectively. The values of PNG-2 and PNG-3 are 50% and 38% higher than the one of PNG-1. These results agree with the piezoelectric output performance in Fig. 6. Especially, PNG-2 and PNG-3 demonstrate the potential as self-powered sensors.

Supplementary material related to this article can be found online at doi:10.1016/j.nanoen.2019.01.022.

4. Conclusions

In this study, PEDOT-C_4:DS and PEDOT-C_6:DS obtained through oxidative polymerization featured nanofiber-type one-dimensional structures. The surface of the casted film demonstrated a similar surface energy (19.7–22.94 mN m^{-1}) to that of PVDF due to its hydrophobicity. PEDOT-C_4:DS demonstrated the highest electrical conductivity (50.0 S cm^{-1}) and PNG-2 showed maximum piezoelectric output power (63.0 nW) at 9 MΩ owing to the high conductive nanofibrillar network, the highly ordered edge-on orientation and dielectric constant (6.74). In contrast, PNG-3 with PEDOT-C_6:DS, a relatively low electrical conductivity (2.7 S/cm) also demonstrated a similar maximum output power (59.9 nW) at 9 MΩ owing to its relatively high electrical homogeneity, dielectric constant (3.69) and Young's modulus (50.49 MPa). Hydrophobic organic electrodes obtained through this study will likely largely contribute to enhancing the performance of organic piezoelectric materials.

Acknowledgements

This research was supported by the New & Renewable Energy Core Technology Program of the Korea Institute of Energy Technology Evaluation and Planning (KETEP) grant funded by the Ministry of Trade, Industry and Energy, Republic of Korea (no. 20153010140030) and the Human Resources Program in Energy Technology of the Korea Institute of Energy Technology Evaluation and Planning (KETEP), granted financial resource from the Ministry of Trade, Industry and Energy, Republic of Korea (No. 20174010201540) and the Korea Institute of Energy Technology Evaluation and Planning (KETEP) and the Ministry of Trade, Industry & Energy (MOTIE) of the Republic of Korea (2018201010636A).

Appendix A. Supporting information

Supplementary data associated with this article can be found in the online version at doi:10.1016/j.nanoen.2019.01.022.

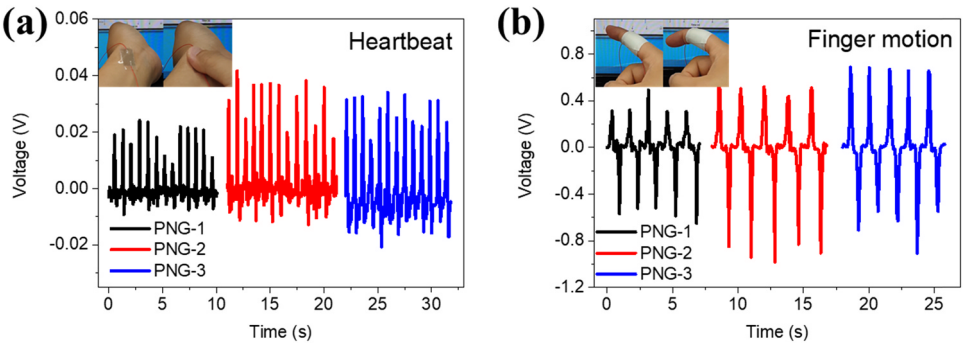

Fig. 8. The generated output voltage performance from the PNGs used for heartbeat monitoring system attached to wrist (a) and human motion monitoring system attached to index finger (b).

References

[1] Y. Hu, Z.L. Wang, Recent progress in piezoelectric nanogenerators as a sustainable power source in self-powered systems and active sensors, Nano Energy 14 (2015) 3–14, https://doi.org/10.1016/j.nanoen.2014.11.038.

[2] X. He, Y. Zi, H. Yu, S.L. Zhang, J. Wang, W. Ding, H. Zou, W. Zhang, C. Lu, Z.L. Wang, An ultrathin paper-based self-powered system for portable electronics and wireless human-machine interaction, Nano Energy 39 (2017) 328–336, https://doi.org/10.1016/j.nanoen.2017.06.046.

[3] Z.L. Wang, Self-powered nanosensors and nanosystems, Adv. Mater. 24 (2012) 280–285, https://doi.org/10.1002/adma.201102958.

[4] K.B. Kim, J.Y. Cho, J. Hamid, J.H. Ahn, S. Do Hong, S.B. Woo, T.H. Sung, Optimized composite piezoelectric energy harvesting floor tile for smart home energy management, Energy Convers. Manag. 171 (2018) 31–37, https://doi.org/10.1016/j.enconman.2018.05.031.

[5] M.H. Choi, E.J. Lee, Y.W. Han, D.K. Moon, Enhancement of the air-stability and optimization of V_{OC} by changing molecular conformation of polyelectrolytes, J. Ind. Eng. Chem. 63 (2018) 426–436, https://doi.org/10.1016/j.jiec.2018.03.003.

[6] T.H. Lee, D.H. Kim, E.J. Lee, D.K. Moon, Significant impact of monomer curvatures for polymer curved shape composition on backbone orientation and solar cell performances, J. Ind. Eng. Chem. 65 (2018) 195–204, https://doi.org/10.1016/j.jiec.2018.04.029.

[7] S.J. Jeon, T.H. Lee, Y.W. Han, D.K. Moon, Design and synthesis of 2D A_1-π-A_2 copolymers impact on fullerene network for efficient polymer solar cells, Polymer 149 (2018) 85–95, https://doi.org/10.1016/j.polymer.2018.04.032.

[8] J.H. Lee, H.J. Yoon, T.Y. Kim, M.K. Gupta, J.H. Lee, W. Seung, H. Ryu, S.W. Kim, Micropatterned P(VDF-TrFE) film-based piezoelectric nanogenerators for highly sensitive self-powered pressure sensors, Adv. Funct. Mater. 25 (2015) 3203–3209, https://doi.org/10.1002/adfm.201500856.

[9] S. Xu, Y. Qin, C. Xu, Y. Wei, R. Yang, Z.L. Wang, Self-powered nanowire devices, Nat. Nanotechnol. 5 (2010) 366–373, https://doi.org/10.1038/nnano.2010.46.

[10] J. Chun, N.R. Kang, J.Y. Kim, M.S. Noh, C.Y. Kang, D. Choi, S.W. Kim, Z. Lin Wang, J. Min Baik, Highly anisotropic power generation in piezoelectric hemispheres composed stretchable composite film for self-powered motion sensor, Nano Energy 11 (2015) 1–10, https://doi.org/10.1016/j.nanoen.2014.10.010.

[11] M.S. Woo, J.H. Ahn, J.H. Eom, W.S. Hwang, J.H. Kim, C.H. Yang, G.J. Song, S. Do Hong, J.P. Jhun, T.H. Sung, Study on increasing output current of piezoelectric energy harvester by fabrication of multilayer thick film, Sens. Actuators A Phys. 269 (2018) 524–534, https://doi.org/10.1016/j.sna.2017.12.025.

[12] K.-I. Park, S. Xu, Y. Liu, G.-T. Hwang, S.-J.L. Kang, Z.L. Wang, K.J. Lee, Piezoelectric $BaTiO_3$ thin film nanogenerator on plastic substrates, Nano Lett. 10 (2010) 4939–4943, https://doi.org/10.1021/nl102959k.

[13] W.S. Jung, M.G. Kang, H.G. Moon, S.H. Baek, S.J. Yoon, Z.L. Wang, S.W. Kim, C.Y. Kang, High output piezo/triboelectric hybrid generator, Sci. Rep. 5 (2015) 1–6, https://doi.org/10.1038/srep09309.

[14] W.S. Jung, M.J. Lee, M.G. Kang, H.G. Moon, S.J. Yoon, S.H. Baek, C.Y. Kang, Powerful curved piezoelectric generator for wearable applications, Nano Energy 13 (2015) 174–181, https://doi.org/10.1016/j.nanoen.2015.01.051.

[15] E.J. Ko, E.J. Lee, M.H. Choi, T.H. Sung, D.K. Moon, PVDF based flexible piezoelectric nanogenerators using conjugated polymer:PCBM blend systems, Sensors Actuatorspolymer: PCBM blend systems, Sens. Actuators A Phys. 259 (2017) 112–120, https://doi.org/10.1016/j.sna.2017.03.013.

[16] J. Kim, J.H. Lee, H. Ryu, J.H. Lee, U. Khan, H. Kim, S.S. Kwak, S.W. Kim, High-performance piezoelectric, pyroelectric, and triboelectric nanogenerators based on P(VDF-TrFE) with controlled crystallinity and dipole alignment, Adv. Funct. Mater. 27 (2017) 1700702, https://doi.org/10.1002/adfm.201700702.

[17] P. Talemi, M. Delaigue, P. Murphy, M. Fabretto, Flexible polymer-on-polymer architecture for piezo/pyroelectric energy harvesting, ACS Appl. Mater. Interfaces 7 (2015) 8465–8471, https://doi.org/10.1021/am5089082.

[18] Z. Zhang, C. Yao, Y. Yu, Z. Hong, M. Zhi, X. Wang, Mesoporous piezoelectric polymer composite films with tunable mechanical modulus for harvesting energy from liquid pressure fluctuation, Adv. Funct. Mater. 26 (2016) 6760–6765, https://doi.org/10.1002/adfm.201602624.

[19] C.S. Lee, J. Joo, S. Han, S.K. Koh, Multifunctional transducer using poly (vinylidene fluoride) active layer and highly conducting poly (3,4-ethylenedioxythiophene) electrode: actuator and generator, Appl. Phys. Lett. 85 (2004) 1841–1843, https://doi.org/10.1063/1.1784890.

[20] J.H. Park, G.T. Hwang, S. Kim, J. Seo, H.J. Park, K. Yu, T.S. Kim, K.J. Lee, Flash-induced self-limited plasmonic welding of silver nanowire network for transparent flexible energy harvester, Adv. Mater. 29 (2017) 1603473, https://doi.org/10.1002/adma.201603473.

[21] S. Lim, D. Son, J. Kim, Y.B. Lee, J.K. Song, S. Choi, D.J. Lee, J.H. Kim, M. Lee, T. Hyeon, D.H. Kim, Transparent and stretchable interactive human machine interface based on patterned graphene heterostructures, Adv. Funct. Mater. 25 (2015) 375–383, https://doi.org/10.1002/adfm.201402987.

[22] S.H. Shin, D.H. Park, J.Y. Jung, M.H. Lee, J. Nah, Ferroelectric zinc oxide nanowire embedded flexible sensor for motion and temperature sensing, ACS Appl. Mater. Interfaces 9 (2017) 9233–9238, https://doi.org/10.1021/acsami.7b00380.

[23] S. Liu, S. Ho, F. So, Novel patterning method for silver nanowire electrodes for thermal-evaporated organic light emitting diodes, ACS Appl. Mater. Interfaces 8 (2016) 9268–9274, https://doi.org/10.1021/acsami.6b00719.

[24] C.M. Palumbiny, F. Liu, T.P. Russell, A. Hexemer, C. Wang, P. Müller-Buschbaum, The crystallization of PEDOT:PSS polymeric electrodes probed in situ during printing, Adv. Mater. 27 (2015) 3391–3397, https://doi.org/10.1002/adma.201500315.

[25] A.I. Hofmann, W.T.T. Smaal, M. Mumtaz, D. Katsigiannopoulos, C. Brochon, F. Schütze, O.R. Hild, E. Cloutet, G. Hadziioannou, An alternative anionic polyelectrolyte for aqueous PEDOT dispersions: toward printable transparent electrodes, Angew. Chem. - Int. Ed. 54 (2015) 8506–8510, https://doi.org/10.1002/anie.201503024.

[26] N. Hong, J. Xiao, Y. Li, Y. Li, Y. Wu, W. Yu, X. Qiu, R. Chen, H.-L. Yip, W. Huang, Y. Cao, Unexpected fluorescent emission of graft sulfonated-acetone–formaldehyde lignin and its application as a dopant of PEDOT for high performance photovoltaic and light-emitting devices, J. Mater. Chem. C 4 (2016) 5297–5306, https://doi.org/10.1039/C6TC01170E.

[27] Y. Wu, J. Wang, X. Qiu, R. Yang, H. Lou, X. Bao, Y. Li, Highly efficient inverted perovskite solar cells with sulfonated lignin doped PEDOT as hole extract layer, ACS Appl. Mater. Interfaces 8 (2016) 12377–12383, https://doi.org/10.1021/acsami.6b00084.

[28] Y. Li, M. Liu, Y. Li, K. Yuan, L. Xu, W. Yu, R. Chen, X. Qiu, H.L. Yip, Poly(3,4-ethylenedioxythiophene): methylnaphthalene sulfonate formaldehyde condensate: the effect of work function and structural homogeneity on hole injection/extraction properties, Adv. Energy Mater. 7 (2017) 1601499, https://doi.org/10.1002/aenm.201601499.

[29] M. Horikawa, T. Fujiki, T. Shirosaki, N. Ryu, H. Sakurai, S. Nagaoka, H. Ihara, The development of a highly conductive PEDOT system by doping with partially crystalline sulfated cellulose and its electric conductivity, J. Mater. Chem. C 3 (2015) 8881–8887, https://doi.org/10.1039/C5TC02074C.

[30] T. Park, B. Kim, Y. Kim, E. Kim, Highly conductive PEDOT electrodes for harvesting dynamic energy through piezoelectric conversion, J. Mater. Chem. A 2 (2014) 5462–5469, https://doi.org/10.1039/C3TA14726F.

[31] Z. Yin, Q. Zheng, Controlled synthesis and energy applications of one-dimensional conducting polymer nanostructures: an overview, Adv. Energy Mater. 2 (2012) 179–218, https://doi.org/10.1002/aenm.201100560.

[32] T.H. Lee, K. Do, Y.W. Lee, S.S. Jeon, C. Kim, J. Ko, S.S. Im, High-performance dye-sensitized solar cells based on PEDOT nanofibers as an efficient catalytic counter electrode, J. Mater. Chem. 22 (2012) 21624, https://doi.org/10.1039/c2jm34807a.

[33] M.G. Han, S.H. Foulger, Facile synthesis of poly(3,4-ethylenedioxythiophene) nanofibers from an aqueous surfactant solution, Small 2 (2006) 1164–1169, https://doi.org/10.1002/smll.200600135.

[34] T.Y. Kim, T.K. Lee, B.S. Kim, S.C. Park, S. Lee, S.S. Im, J. Bisquert, Y.S. Kang, Triumphing over charge transfer limitations of PEDOT nanofiber reduction catalyst by 1,2-ethanedithiol doping for quantum dot solar cells, ACS Appl. Mater. Interfaces 9 (2017) 1877–1884, https://doi.org/10.1021/acsami.6b12536.

[35] T. Ji, L. Tan, X. Hu, Y. Dai, Y. Chen, A comprehensive study of sulfonated carbon materials as conductive composites for polymer solar cells, Phys. Chem. Chem. Phys. 17 (2015) 4137–4145, https://doi.org/10.1039/C4CP04965A.

[36] W. Zhang, B. Zhao, Z. He, X. Zhao, H. Wang, S. Yang, H. Wu, Y. Cao, High-efficiency ITO-free polymer solar cells using highly conductive PEDOT:PSS/surfactant bilayer transparent anodes, Energy Environ. Sci. 6 (2013) 1956, https://doi.org/10.1039/c3ee41077c.

[37] T.Y. Kim, W. Wei, T.K. Lee, B.S. Kim, S.C. Park, S. Lee, E.H. Suh, J. Jang, J. Bisquert, Y.S. Kang, Imidazolium iodide-doped PEDOT nanofibers as conductive catalysts for highly efficient solid-state dye-sensitized solar cells employing polymer electrolyte, ACS Appl. Mater. Interfaces 10 (2018) 2537–2545, https://doi.org/10.1021/acsami.7b16017.

[38] Y.H. Kim, C. Sachse, M.L. MacHala, C. May, L. Müller-Meskamp, K. Leo, Highly conductive PEDOT:PSS electrode with optimized solvent and thermal post-treatment for ITO-free organic solar cells, Adv. Funct. Mater. 21 (2011) 1076–1081, https://doi.org/10.1002/adfm.201002290.

[39] Y. Xia, K. Sun, J. Ouyang, Highly conductive poly(3,4-ethylenedioxythiophene):poly(styrene sulfonate) films treated with an amphiphilic fluoro compound as the transparent electrode of polymer solar cells, Energy Environ. Sci. 5 (2012) 5325–5332, https://doi.org/10.1039/C1EE02475B.

[40] N.K. Unsworth, I. Hancox, C. Argent Dearden, P. Sullivan, M. Walker, R.S. Lilley, J. Sharp, T.S. Jones, Comparison of dimethyl sulfoxide treated highly conductive poly(3,4-ethylenedioxythiophene):poly(styrenesulfonate) electrodes for use in indium tin oxide-free organic electronic photovoltaic devices, Org. Electron. Phys. Mater. Appl. 15 (2014) 2624–2631, https://doi.org/10.1016/j.orgel.2014.07.015.

[41] M. Annamalai, K. Gopinadhan, S.A. Han, S. Saha, H.J. Park, E.B. Cho, B. Kumar, A. Patra, S.-W. Kim, T. Venkatesan, Surface energy and wettability of van der Waals structures, Nanoscale 8 (2016) 5764–5770, https://doi.org/10.1039/C5NR06705G.

[42] M. Okouchi, Y. Yamaji, K. Yamauchi, Contact angle of poly(alkyl methacrylate)s and effects of the alkyl group, Macromolecules 39 (2006) 1156–1159, https://doi.org/10.1021/ma052168g.

[43] J.Y. Oh, M. Shin, J.B. Lee, J.H. Ahn, H.K. Baik, U. Jeong, Effect of PEDOT nanofibril networks on the conductivity, flexibility, and coatability of PEDOT:PSS films, ACS Appl. Mater. Interfaces 6 (2014) 6954–6961, https://doi.org/10.1021/am500769k.

[44] X. Hou, Q. Li, T. Cheng, L. Yu, F. Wang, J. Lin, S. Dai, Y. Li, Z. Tan, Improvement of the power conversion efficiency and long term stability of polymer solar cells by incorporation of amphiphilic Nafion doped PEDOT-PSS as a hole extraction layer, J. Mater. Chem. A 3 (2015) 18727–18734, https://doi.org/10.1039/C5TA03967C.

[45] Y. Zhang, L. Chen, X. Hu, L. Zhang, Y. Chen, Low work-function Poly(3,4-ethylenedioxylenethiophene): poly(styrene sulfonate) as electron-transport layer for high-efficient and stable polymer solar cells, Sci. Rep. 5 (2015) 1–12, https://doi.org/10.1038/srep12839.

[46] D.J. Beesley, J. Semple, L. Krishnan Jagadamma, A. Amassian, M.A. McLachlan, T.D. Anthopoulos, J.C. Demello, Sub-15-nm patterning of asymmetric metal electrodes and devices by adhesion lithography, Nat. Commun. 5 (2014) 1–9, https://doi.org/10.1038/ncomms4933.

[47] J. a. Merlo, C.D. Frisbie, Field effect conductance of conducting polymer nanofibers,

J. Polym. Sci. Part B - Polym. Phys. 41 (2003) 2674, https://doi.org/10.1002/polb.10656.
[48] M.Y. Teo, N. Kim, S. Kee, B.S. Kim, G. Kim, S. Hong, S. Jung, K. Lee, Highly stretchable and highly conductive PEDOT:PSS/Ionic liquid composite transparent electrodes for solution-processed stretchable electronics, ACS Appl. Mater. Interfaces 9 (2017) 819–826, https://doi.org/10.1021/acsami.6b11988.
[49] L. Persano, C. Dagdeviren, Y. Su, Y. Zhang, S. Girardo, D. Pisignano, Y. Huang, J.A. Rogers, High performance piezoelectric devices based on aligned arrays of nanofibers of poly(vinylidenefluoride-co-trifluoroethylene), Nat. Commun. 4 (2013) 1–10, https://doi.org/10.1038/ncomms2639.
[50] E. Kabir, M. Khatun, L. Nasrin, M.J. Raihan, M. Rahman, Pure β-phase formation in polyvinylidene fluoride (PVDF)-carbon nanotube composites, J. Phys. D. Appl. Phys. 50 (2017) 163002, https://doi.org/10.1088/1361-6463/aa5f85.
[51] Y.W. Su, Y.C. Lin, K.H. Wei, Evolving molecular architectures of donor-acceptor conjugated polymers for photovoltaic applications: from one-dimensional to branched to two-dimensional structures, J. Mater. Chem. A 5 (2017) 24051–24075, https://doi.org/10.1039/c7ta07228g.
[52] L. Feng, F. Zheng, P.Q. Bi, X.Y. Yang, M.S. Niu, F. Wang, X.T. Hao, Laser-induced crystallization and conformation control of poly(3-hexylthiophene) for improving the performance of organic solar cells, Org. Electron. Phys. Mater. Appl. 49 (2017) 157–164, https://doi.org/10.1016/j.orgel.2017.06.053.
[53] C. Wan, C.R. Bowen, Multiscale-structuring of polyvinylidene fluoride for energy harvesting: the impact of molecular-, micro- and macro-structure, J. Mater. Chem. A 5 (2017) 3091–3128, https://doi.org/10.1039/c6ta09590a.
[54] J.-H. Lee, K.Y. Lee, B. Kumar, N.T. Tien, N.-E. Lee, S.-W. Kim, Highly sensitive stretchable transparent piezoelectric nanogenerators, Energy Environ. Sci. 6 (2013) 169–175, https://doi.org/10.1039/C2EE23530G.
[55] R. Ding, X. Zhang, G. Chen, H. Wang, R. Kishor, J. Xiao, F. Gao, K. Zeng, X. Chen, X.W. Sun, Y. Zheng, High-performance piezoelectric nanogenerators composed of formamidinium lead halide perovskite nanoparticles and poly(vinylidene fluoride), Nano Energy 37 (2017) 126–135, https://doi.org/10.1016/j.nanoen.2017.05.010.
[56] J. Yan, Y.G. Jeong, High performance flexible piezoelectric nanogenerators based on BaTiO3Nanofibers in different alignment modes, ACS Appl. Mater. Interfaces 8 (2016) 15700–15709, https://doi.org/10.1021/acsami.6b02177.
[57] S. Jana, S. Garain, S. Sen, D. Mandal, The influence of hydrogen bonding on the dielectric constant and the piezoelectric energy harvesting performance of hydrated metal salt mediated PVDF films, Phys. Chem. Chem. Phys. 17 (2015) 17429–17436, https://doi.org/10.1039/c5cp01820j.
[58] M. Sharma, V. Srinivas, G. Madras, S. Bose, Outstanding dielectric constant and piezoelectric coefficient in electrospun nanofiber mats of PVDF containing silver decorated multiwall carbon nanotubes: assessing through piezoresponse force microscopy, RSC Adv. 6 (2016) 6251–6258, https://doi.org/10.1039/C5RA25671B.
[59] V. Bhavanasi, V. Kumar, K. Parida, J. Wang, P.S. Lee, Enhanced piezoelectric energy harvesting performance of flexible PVDF-TrFE bilayer films with graphene oxide, ACS Appl. Mater. Interfaces 8 (2016) 521–529, https://doi.org/10.1021/acsami.5b09502.
[60] V. Cauda, S. Stassi, A. Lamberti, M. Morello, C. Fabrizio Pirri, G. Canavese, Leveraging ZnO morphologies in piezoelectric composites for mechanical energy harvesting, Nano Energy 18 (2015) 212–221, https://doi.org/10.1016/j.nanoen.2015.10.021.
[61] C. Yan, W. Deng, L. Jin, T. Yang, Z. Wang, X. Chu, H. Su, J. Chen, W. Yang, Epidermis-inspired ultrathin 3D cellular sensor array for self-powered biomedical monitoring, ACS Appl. Mater. Interfaces 10 (2018) 41070–41075, https://doi.org/10.1021/acsami.8b14514.
[62] X. Chen, J. Shao, N. An, X. Li, H. Tian, C. Xu, Y. Ding, Self-powered flexible pressure sensors with vertically well-aligned piezoelectric nanowire arrays for monitoring vital signs, J. Mater. Chem. C 3 (2015) 11806–11814, https://doi.org/10.1039/c5tc02173a.
[63] W. Deng, T. Yang, L. Jin, C. Yan, H. Huang, X. Chu, Z. Wang, D. Xiong, G. Tian, Y. Gao, H. Zhang, W. Yang, Cowpea-structured PVDF/ZnO nanofibers based flexible self-powered piezoelectric bending motion sensor towards remote control of gestures, Nano Energy 55 (2019) 516–525, https://doi.org/10.1016/j.nanoen.2018.10.049.
[64] S. Siddiqui, D. Il Kim, L.T. Duy, M.T. Nguyen, S. Muhammad, W.S. Yoon, N.E. Lee, High-performance flexible lead-free nanocomposite piezoelectric nanogenerator for biomechanical energy harvesting and storage, Nano Energy 15 (2015) 177–185, https://doi.org/10.1016/j.nanoen.2015.04.030.
[65] L. Jin, S. Ma, W. Deng, Y. Cheng, T. Yang, X. Chu, G. Tian, D. Xiong, J. Lu, W. Yang, Polarization-free high-crystallization β-PVDF piezoelectric nanogenerator toward self-powered 3D acceleration sensor, Nano Energy 50 (2018) 632–638, https://doi.org/10.1016/j.nanoen.2018.05.068.

Eui Jin Ko received his B.S. degree from the Department of Materials Chemistry and Engineering, Konkuk University, Korea in 2012. He is currently a Ph.D. candidate in the Nano & Information Materials Laboratory, Department of Chemical Engineering, Konkuk University, Republic of Korea under Prof. Doo Kyung Moon's supervision. His research interests are in conducting polymers and piezoelectric nanogenerators.

Sung Jae Jeon received his B.S. degree from the Department of Materials and Chemistry Engineering, Konkuk University, Republic of Korea in 2013. He is currently a Ph.D. candidate in the Nano & Information Materials Laboratory (NIMs), Department of Chemical Engineering, Konkuk University, Republic of Korea working under the supervision of Prof. Doo Kyung Moon. His research focuses on designing and synthesizing conjugated materials with high-performance for organic electronics.

Yong Woon Han received his B.S. degree from the Department of Materials and Chemistry Engineering, Konkuk University, Republic of Korea in 2013. He is currently a Ph.D. candidate in the Nano & Information Materials Laboratory, Department of Chemical Engineering, Konkuk University, Republic of Korea under Prof. Doo Kyung Moon's supervision. His research interests focuses on the developing structure and mechanism of organic-in-organic hybrid solar cells.

Se yeong Jeong received his B.Sc. in 2014 Electronic in Engineering from Seoul National University of Science and Technology, Seoul, South Korea. He is pursuing M.Sc & Ph.D. integrated course under direction of Professor Tae-Hyun Sung at the Department of Electrical Engineering, Hanyang University. His research interests include optimization of energy harvesting system and circuit designing for Application.

Chong Yun Kang received his B.S. degree (1993), M.S. degree (1995) and Ph.D. degree (2000) from Yonsei University. He was in the University of Birmingham in UK as a post-doc (2002–2004), and in UCLA in USA as a visiting scholar (2008). Since 2000, he is a principal research scientist in Korea Institute of Science and Technology (KIST). Since 2012, he is a professor in KU-KIST Graduate School in Korea University. His research interests include piezoelectric and triboelectric energy harvesters, and metal oxide semiconductor gas sensors.

Tae Hyun Sung received a B.A. (1982), an M.S. (1987) in inorganic material engineering from Hanyang University and a Ph.D. (1991) in Material Science and Engineering from Tokyo Institute of Technology. He worked at International Superconductivity Technology Center (ISTEC) as a researcher (1992). He was in Massachusetts Institute of Technology (MIT) as a Post doc. (1995). He worked at the Korea Electric Power Research Institute (KEPRI) as a group leader of superconductivity group. Also, he was selected as a "Top 100 Engineers" by IBC (International Biographic Center), is the member of the National Academy of Engineering of Korea (NAEK). Since 2009, he has been professor of Department of Electrical Engineering, Hanyang University. His research interests include superconductivity, electrical material, energy storage device, and piezoelectric energy harvesting technology.

Kee Won Seong received his B.S. degree (1988), M.S. degree (1990) and Ph.D. degree (1994) from Seoul National University. He had worked for Korea Institute of Construction Technology (KICT, 1994–1997) as a senior researcher leading a team dealing natural disaster with statistics. He has studied soft computing application in various engineering field after a visiting professor experience in the University of New South Wales (UNSW, 2006–2007). He has been a professor of Konkuk University since 1998. His recent research focus on a multi-method framework for support natural energy harvesting method,

Doo Kyung Moon received his Ph.D. from Tokyo Institute of Technology, Japan in 1993, and had post-doc experience at the University Arizona in USA (1993–1994) and the Korea Institute of Science and Technology (KIST, 1994–1995). Now, he is a professor of the Department of Chemical Engineering, Konkuk University, Republic of Korea. He was an adjunct professor of Advanced Industrial Science and Technology (AIST, 2009–2010). His research group works on the development of organic materials and organic electronic devices for organic solar cells, organic light emitting diodes and piezoelectric nanogenerators. For details please see the lab website: http://nanoscience.or.kr